EASR

Engineering and Applied Science Research

https://www.tci-thaijo.org/index.php/easr/index

Published by the Faculty of Engineering, Khon Kaen University, Thailand

Insight into molecular weight cut off characteristics and reduction of melanoidin using microporous and mesoporous adsorbent

Kowit Suwannahong[1)], Surachai Wongcharee*[2)], Javier Rioyo[3)], Chadrudee Sirilamduan[4)] and Torpong Kreetachart[5)]

[1)]Department of Environmental Health, Faculty of Public Health, Burapha University, Chonburi 20131, Thailand
[2)]Field of Environmental Engineering, Faculty of Engineering, Mahasarakham University, Mahasarakham 44150, Thailand
[3)]Department of Environmental Engineering, Condorchem Envitech, Barcelona, Spain
[4)]Department of Business Management, Faculty of Management Science, Ubon Ratchathani University, Ubon Ratchathani 34150, Thailand
[5)]Department of Environmental Engineering, School of Energy and Environment, University of Phayao, Phayao 56000, Thailand

Received 15 March 2021
Revised 2 May 2021
Accepted 18 May 2021

Abstract

A detailed breakdown of synthetic melanoidin at the fractionations of molecular cut off points of 10kDa, 5kDa and 1kDa using sterlitech ultrafiltration membranes had been conducted by applying DOC, pH, UV-vis$_{254}$, SSAC$_{346}$, FTIR and EEMs as a surrogate parameter to examine the structural fractioned melanoidin and favored specific pore size of the adsorption process. At room temperature, pH did not have any specific changes subsequent to fractionation. DOC, UV$_{254}$ and SSAC$_{436}$ were significantly increased for a higher MWCO fraction in the order 5-10kDa, 1-5kDa and <1kDa, respectively. Multifunctional groups of fractioned melanoidin at different fractionation groups were found to react easily with the hydroxyl functional group present in the carbon material surface, likely contributing to the adsorption. Using EEMs (excitation-emission 3-dimensional matrices), the spectra showed that at the different fractionations of melanoidin, peaks of fulvic acid-like materials and humic acid-like organic materials corresponding to the Ex/Em regions of 237-260/400-500 nm and 300-370/400-500 nm, belonged to tryptophan and protein-like compounds. The sorption behaviors were all well-fitted to Langmuir isotherm with physisorption of maximum melanoidin adsorbed about 17.88 mg melanoidin g^{-1} (<1kDa) and about 23.71 mg melanoidin g^{-1} (5-10kDa) for micropore and mesoporous adsorbent respectively. The above confirmed that the MWCO affected the adsorption process mechanism due to a mass balance transfer between solution bulk density concentration and porous structure. These results may be able to provide clues to evaluate the role of the elimination of recalcitrant melanoidin in wastewater and other specific purposes using suitable adsorbent material for particular molecular weight cut off points.

Keywords: Adsorption, Microporous and mesoporous, Melanoidin, Fractionation, EEMs

1. Introduction

Melanoidin (Molasses Spent Wash, MSW) is well known as a negatively charged that produces coloured and/or macromolecules as final products of Maillard reaction [1]. Melanoidin reaction products contribute to the colour formation of dark brown polymeric compounds, which arise from the chemical reaction of parallel non-enzymatic such as amino acid compounds, peptides and proteins of organic matter [2, 3]. These reactions are observed during fermentation and/or the distillation processing of food products such as bakery yeast, coffee, brewery malt, beef and ethanol production [3-5]. These polymerization degrees can produce a dark brown colour due to a high organic load in the effluent [6, 7], which is closely related to melanin, lipofuscin, tannic pigment, humic substances, lignin, coal tar and caramel [8]. However, it depends on the reactants and concentrations of reaction conditions [9] such as those in the soil and foods and *in vivo* [10]. It can also be easily be distributed in various aquatic ecosystems such as oceans, lakes, rivers, streams, estuaries and wetlands. The antioxidant properties of Melanoidin can cause problems for many organisms in water and wastewater treatment such as the reduction of photosynthesis, reduction of alkalinity, reduction of sunlight penetration, manganese availability and inhibition of seed germination [11, 12]. Melanoidins have an empirical formula of $C_{17\text{-}18}H_{26\text{-}27}O_{10}N$ (Figure 1) around 5-40kDA of molecular weight distribution [13], and the structural information and characteristics of melanoidin are still poorly defined by supported data [14]. Melanoidin acts as net negatively charged anionic hydrophilic polymers that can form a stable complex with metal cation ions such as copper, chromium, iron, zinc, lead, etc. [15, 16]. Various methods for removing the colour associated with melanoidin have been well reported in the literature. Several conventional techniques have been used to eliminate the decolorisation of melanoidin from wastewater effluent: physicochemical treatment, biological degradation treatment, membrane technologies and application of the electrochemical method which possesses high treatment performance [17]. These techniques are employed widely with the goal of reducing organic loads and colour from the wastewater effluent.

Biological treatment/advanced biological treatment is widely used to remove organic loads from wastewater effluent such as the sewage treatment plant due to it is rich in brown nitrogen polymer associated with melanoidin [3]. Research findings report that

*Corresponding author. Tel.: +66 8662 0962
Email address: surachai.wongcharee@outlook.com
doi: 10.14456/easr.2022.5

municipal wastewater from sewage treatment plants can treat around 20 mL day^{-1} of molasses final product streams [18]. However, unpleasant colour and other biologically recalcitrant organic compounds of treated melanoidin are remain in high COD and DON levels that cannot be eliminated by advanced biological treatment. It is well known that advanced oxidation processes may take away the intractable melanoidin to a certain degree, however no unique technology has proved to be successful in eliminating the remaining melanoidin from wastewater associated with melanoidin [19]. Therefore, high-performance pre-treatment, degradation and decolonization for wastewater associated with melanoidin should be performed by continuing with other processes such as adsorption or chemical methods.

Many scientists have investigated specific porous materials such as activated carbon in various applications for water and wastewater treatment processes. The application of porous materials such as microporous, mesoporous and macroporous is appealing in many fields of research as pore sizes are close to those of biological macromolecules, which have a significant impact on the adsorption mechanism [19] in water and wastewater treatment. However, the separation of material immediately after the end treatment process should be explored due to the separation of particles in the conventional treatment plant being a high cost and time consuming operation [20]. As a result, specific porous materials have been extensively examined for multiple applications in water and wastewater treatment. Several applications of microporous and mesoporous materials for the adsorption of compounds such as gas [21, 22], ammonium [23, 24], heavy metals [25], drugs [26], methylene blue [27, 28], organic dye [29, 30], CO_2, [31, 32], n-heptane, toluene, o-xylene [33] and other water pollutants [34, 35] with different outcomes from aqueous solutions have been published in the literature. Therefore, using materials with a specific pore size would be effective in the elimination of wastewater effluent associated with melanoidin. The adsorption process is an alternative choice that is commonly used in the treatment of wastewater effluent associated with melanoidin, which is an effective method with no by-products emissions. Therefore, it could be useful to examine the application of structural fractioned melanoidin in the adsorption process with a specific pore size.

The primary objective of this scientific research was to examine the removal of melanoidin from water using specific micro and mesoporous activated carbon as an adsorbent. The effect of pore size was investigated through fractioned melanoidin in serial fractionation using 10kDa, 5kDa, and 1kDa sterlitech ultrafiltration membranes. Moreover, adsorption capacity and isotherm (Langmuir and Freundlich) behaviors of the specific micro- and mesoporous materials were examined in the sorption process through a batch testing experiment using nonlinear regression to determine process parameters.

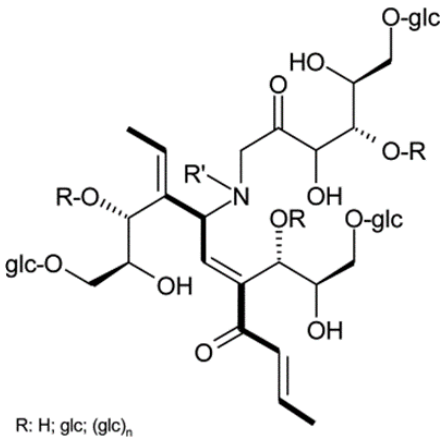

Figure 1 The chemical structure of melanoidin formed in the Maillard reaction [36]

2. Materials and methods

2.1 Adsorbent and synthetic melanoidin preparation

Mesoporous materials know as powdered activated carbon that were obtained from residual macadamia nut shell were prepared using carbon dioxide gas as an activating agent from 30 ºC to 900 ºC over 1 h. Microporous activated carbon/commercial activated carbon was supplied by the Clarence Water Company, Australia and made from coconut shell. Both adsorbents were milled using Ball Miller (Pulverisette 5, Fritsch) to form powdered activated carbon and washed with double water at 120 ºC for over 12 h. The physical and chemical properties have been described in depth in the literature [37]. The synthetic solution of melanoidin was prepared by following the literature [38], combining of 60 ml double water with about 0.42 g sodium bicarbonate from 4.5 g glucose and 1.88 g glycine. The combined solution was mixed until dissolved by adding double water up to 100 ml. The completely mixed solution was boiled at 95 ℃ for about 7 h to achieve a rich brown aliquot. The obtained concentrated synthetic melanoidin aliquots were diluted to a maximum of 250 mL using double water and were kept at 4 ℃ in the control temperature fridge for further analysis and characterization [3].

2.2 Fractioned melanoidin

Figure 2 presents the step to obtain the fractioned melanoidin of >10kDa, 5-10kDa, 1-5kDa and <1kDa molecular weight fraction. Diluted original melanoidin of 1000 mL used in serial fractionation was prepared using aliquots of 20 mL of synthetic melanoidin obtained as described in Section 2.1 with 980 mL of distilled water. The polymeric stirred cell (sterlitech) used in this study has a diameter of about 150 mm acrylic (cell barrel). Sterlitech ultrafiltration membranes with MWCO points of 10kDa, 5kDa, and 1kDa were used and alternated in the serial fractionation after retentate volume of synthetic melanoidin remains of about 250 mL, as shown in Figure 2 for each fractionation. Each fractioned melanoidin was stored in the cold room for further characterization and analysis.

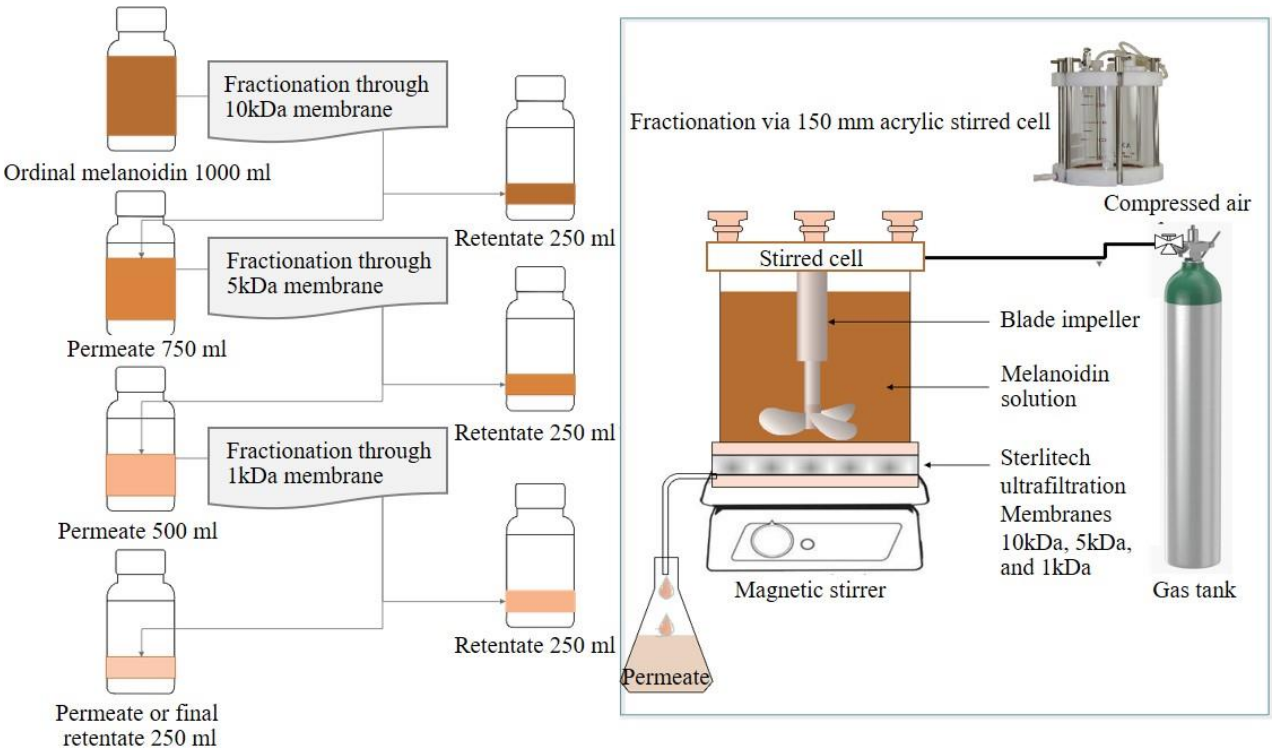

Figure 2 Fractionation steps to obtain the fractioned melanoidin of >10kDa, 5-10kDa, 1-5kDa and < 1kDa molecular weight fraction

2.3 Melanoidin reduction efficiency and equilibrium adsorption

In this study, the DOC (dissolved organic matter) parameter was defined as the melanoidin concentration to explore the ability of adsorption in different porous materials. For melanoidin reduction efficiency, the effect of time and equilibrium adsorption studies were conducted in a batch experiment at neutral pH. A stock solution of melanoidin at different fractionations of >10kDa, 5-10kDa, 1-5kDa and <1kDa molecular weight were prepared from the method defined in Section 2.2 (fractioned melanoidin). Using a 250 mL Erlenmeyer flask with closing parafilm, 50 mL of 0 to 15 mg melanoidin L^{-1} solution with 10 mg of powdered microporous and mesoporous adsorbent were added for the experimental batch testing that was associated with each fractioned melanoidin as mentioned above in Section 2.2. Next, the mixed sample solution was shaken at 140 rpm in a water bath with the temperature controlled at 25 ºC for four days. Then, the mixed solution was filtered via 0.45 µm syringe filters to reach equilibrium. The contact time effect was obtained with 10 mg microporous and mesoporous adsorbent in a similar manner except that the solution was withdrawn during the zero to five day time period in separate runs. Triplicate runs of the experiment for each fractionation, and with a controlled blank solution, was used to establish the precision and reliability of the experimental data. The mass of DOC (named melanoidin) adsorbed q_e (mg g^{-1}) at equilibrium was calculated from the equation:

$$q_e = ((C_0 - C_e)/m) \times V \quad (1)$$

where C_0 (mg melanoidin L^{-1}) is the initial concentration of synthetic melanoidin, C_e (mg melanoidin L^{-1}) is the concentration of synthetic melanoidin at equilibrium, V (L) is the volume of the synthetic melanoidin solution, and m (g) is the mass of the microporous and mesoporous materials used in this study.

2.4 Analysis methodology

To examine the treatment of DOC, aliquot for each fractionation was filtrated via 0.45 µm filter via syringe filters (25 mm diameter) and analyzed through a TOC analyzer (Shimadzu) in order. Fourier-Transformed Infrared (Perkin Elmer Two ATR-FTIR) equipment was applied to recognize the surface functional groups and assess the full range of absorbance, while the obtained pH was measured using a Eutech, PC2700 pH meter and adjusted using a HCl solution (hydrochloric) and NaOH solution (sodium hydroxide) for each fractioned melanoidin. A Shimadzu RF-6000 Fluorescence Spectrophotometer was used to measure the cover range of 200-600 nm intensity of EEMs that were provided as three-dimensional plots. UV-Vis spectrophotometer (Jenway-6715) also was applied to measure the absorbance of synthetic wastewater effluent associated with melanoidin.

3. Results and discussion

3.1 Basic feature of fractioned melanoidin at different fractionations

Figure 3 presents an example of the colour characterization of melanoidin at different fractionations in the order of >10 kDa, 5-10 kDa, 1-5 kDa and <1 kDa molecular weight. It can be observed that the colour concentration of the fractioned melanoidin displayed a decreasing trend from >10kDa followed by 5-10 kDa, 1-5 kDa and < 1 kDa respectively. The basic feature of melanoidin fractionation was investigated via pH, UV_{254}, DOC (TOC analyzer) and colure ($SSAC_{436}$), which were used as surrogate parameters. Figure 4

demonstrates the pH, UV_{254}, DOC and $SSAC_{436}$ results of molecular weight fraction of melanoidin. It can be concluded that pH did not show any specific changes (average around pH 7.54) for all fractions, even the original melanoidin with not more than 3% difference at room temperature (23 ± 0.5 ºC). In terms of DOC, it could be seen that >10kDa indicated a high molecular weight fraction about 254 mg DOC L^{-1} compared to 5-10kDa (175 mg DOC L^{-1}), 1-5kDa (145 mg DOC L^{-1}) and <1kDa (140 mg DOC L^{-1}) respectively. While humic fraction/UV-vis wavelength (UV_{254}) and $SSAC_{436}$ (brown or yellow) were higher for the higher molecular fraction at >10kDa and reducing in the order of 5-10kDa, 1-5kDa and <1kDa followed the DOC results, respectively. It can be seen that the extensive qualitative and quantitative characterization surveys direct on the fractioned melanoidin can be applied in the sorption behavior process [3] for high-quality water and wastewater treatment. Moreover, these results could also be used as basic preliminary information for designing the operating condition in the industrial level of a water treatment plant.

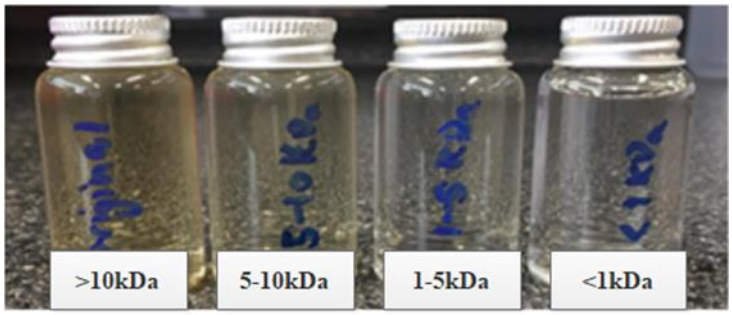

Figure 3 Colour characterization of fractioned melanoidin at different fractionations

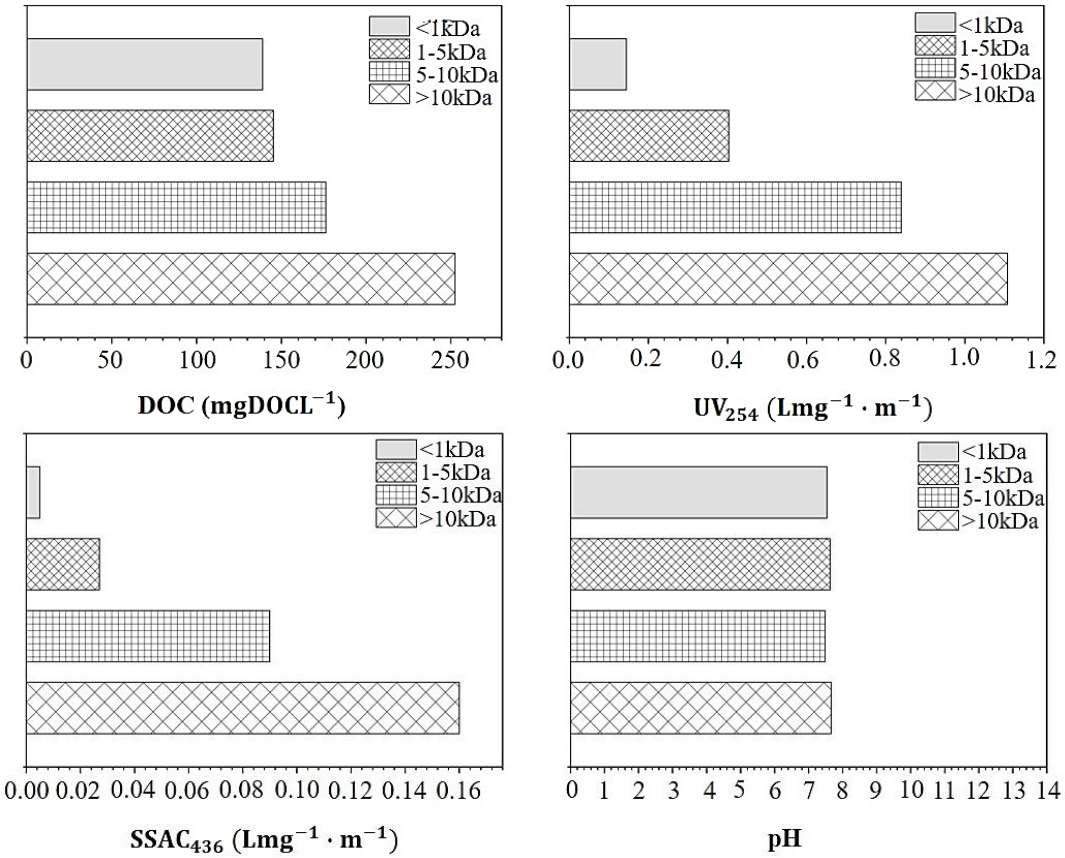

Figure 4 pH, $SSAC_{436}$, DOC and UV_{254} of fractioned melanoidin at different fractionations

3.2 UV-vis spectra and FTIR spectra at different fractionations

Figure 5(a) represents absorbance versus wavelength of UV-vis spectrophotometer and Figure 5(b) displays the characterization of functional groups for fractioned melanoidin at different fractionations. This could be observed that UV-vis spectra was enhanced or decreased after fractionation in the order of >10 kDa, 5-10 kDa, 1-5 kDa and < 1 kDa MWCO. Visual representation was verified as illustrated in up-right inset (2D plot of EEMs) in Figure 5(a), which demonstrates a forceful characterization of dissolved organic matter (DOM, UV_{254}). The dominant peak at 275 nm constitutes the ability to absorb energy for UV-vis spectrum that is related to hydrothermal electrons transfers of melanoidin [39] which can release energy as electromagnetic radiation [40]. The chemical characteristic of surface functional groups for fractioned melanoidin at different fractionations was explored using FTIR spectroscopy. The functional groups are the most important factors in offering affinity and selectivity in the direction of a particular adsorbent for the adsorption process, as shown in Figure 5(b) of the functional groups of fractioned melanoidin at different fractionations. It can be

concluded that the functional groups of fractioned melanoidin had no significant difference for all molecular weight fractions. The FTIR spectra peaks or a broad absorption at 3739 cm^{-1} and 3235 cm^{-1} as shown in Figure 5(b) indicating that can be ascribed to O-H or N-H the stretching vibration and the peak at 2928 cm^{-1} were assigned to aliphatic C-H groups. The peak at 2346 cm^{-1} was ascribed to the stretching vibration to C≡C (alkynes group). The broad peaks at 1601 cm^{-1} indicated that was originated from the double bonds groups of C=O/C=C. The absorbance peak at 1378 cm^{-1} and 1050 cm^{-1} correspond to the alkylamine group (C=N) and stretching vibration of an ether group (C-O-C), respectively. It can be summarized that multifunctional groups of fractioned melanoidin at different fractionation groups can easily react with the hydroxyl functional group (R-O-H) present in the carbon material surface likely contributing to the adsorption process [41].

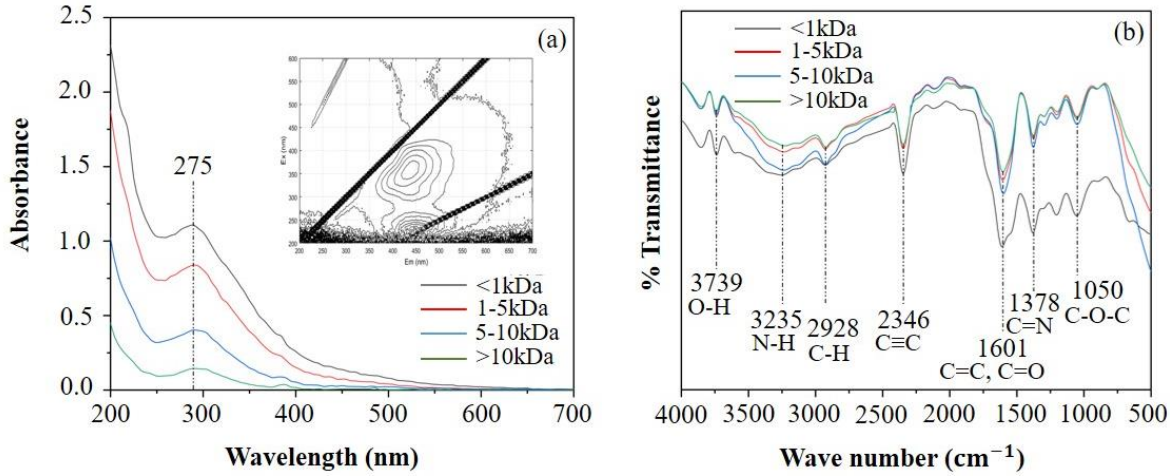

Figure 5 (a) Absorbance versus wavelength of UV-vis spectrophotometer for fractioned melanoidin and (b) Functional groups of fractioned melanoidin at different fractionations

To characterize the DOC used as a surrogate parameter in predicting organic compounds loaded in wastewater associated with melanoidin, a fluorescence EEMs was performed through Fourier-transform spectroscopy. EEMs provide a graph composed of 3-dimensional plots of the intensity of molecular excitation-emission in the UV-visible wavelength range that could be used for supporting the identification of DOC in freshwater sources [42]. Figure 6 shows contour plots of corresponding fluorescence EEMs and displays image plots for each wavelength of >10kDa, 5-10kDa, 1-5kDa and <1kDa MWCO.

The fluorescence regional integration of EEMs spectra is defined into five excitation-emission regions in the horizontal and vertical lines form based on the fluorescence of model compounds such as DOM in surface water of different MWCO fractions including marine water or freshwater [43]. Regions A and B have been associated with the peaks of shorter excitation-emission wavelengths which are related to simple aromatic proteins such as tyrosine [44, 45]. Region C consists of peaks of fulvic acid-like materials [46] and Region D involves peaks of soluble microbial byproduct-like materials [47]. Region E relates peaks at the longer excitation wavelength (>280) and longer emission wavelength (>380) that are associated with humic acid-like organics [48]. As a result, it can be noted that the contour and display image plots of distilled water (blank) had not displayed the peaks for all regions A, B, C, D and E. MWCO at >10kDa, 5-10kDa, 1-5kDa and < kDa showed two distinct peaks in EEMs, indicated as Regions C and E in Figure 6. Region C indicated the peaks of fulvic acid-like materials corresponding to the Ex/Em regions of 237-260/400-500 nm [49] respectively, while the region E peaks demonstrated the humic acid-like organics product materials occurring at Ex/Em of 300-370/400-500 nm [43] belonging to the tryptophan and protein-like compounds. Nevertheless, region peaks situated in lengthier emission the wavelengths more than >600 nm were designated to pigments [50]. However, as shown in Figure 6 did not show any pigment peaks at the lengthier emission the wavelengths more than >600 nm, it might be due to artificial synthetic melanoidin was not real like molasses spent wash effluent. It could be suggested that the MWCO of >10kDa demonstrated high intensity compared to the 5-10kDa, 1-5kDa and <1kDa molecular weight cut off fractions respectively owing to the extreme molecular weight cut off (>10kDa) responding better to the IR-spectrum than the low molecular weight cut off of 5kDa, 1kDa and <1kDa respectively.

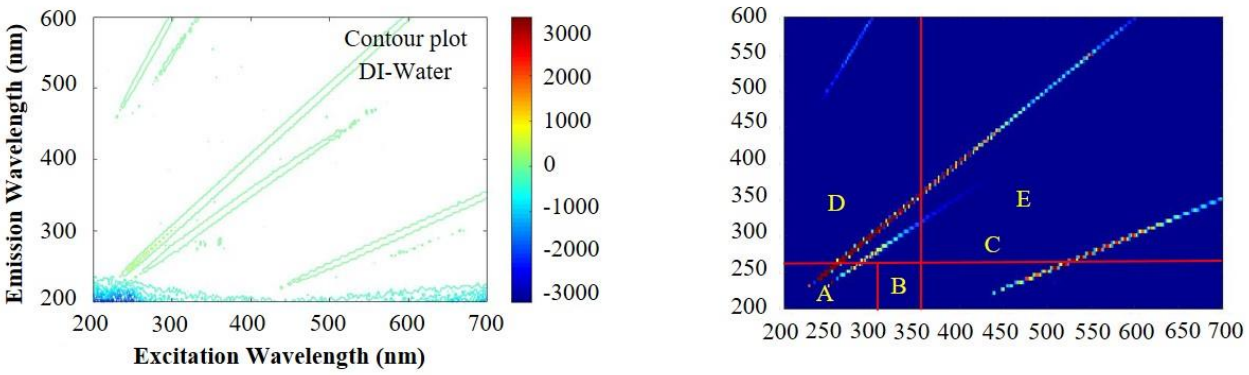

Figure 6 Contour and display image plots for fractioned melanodin

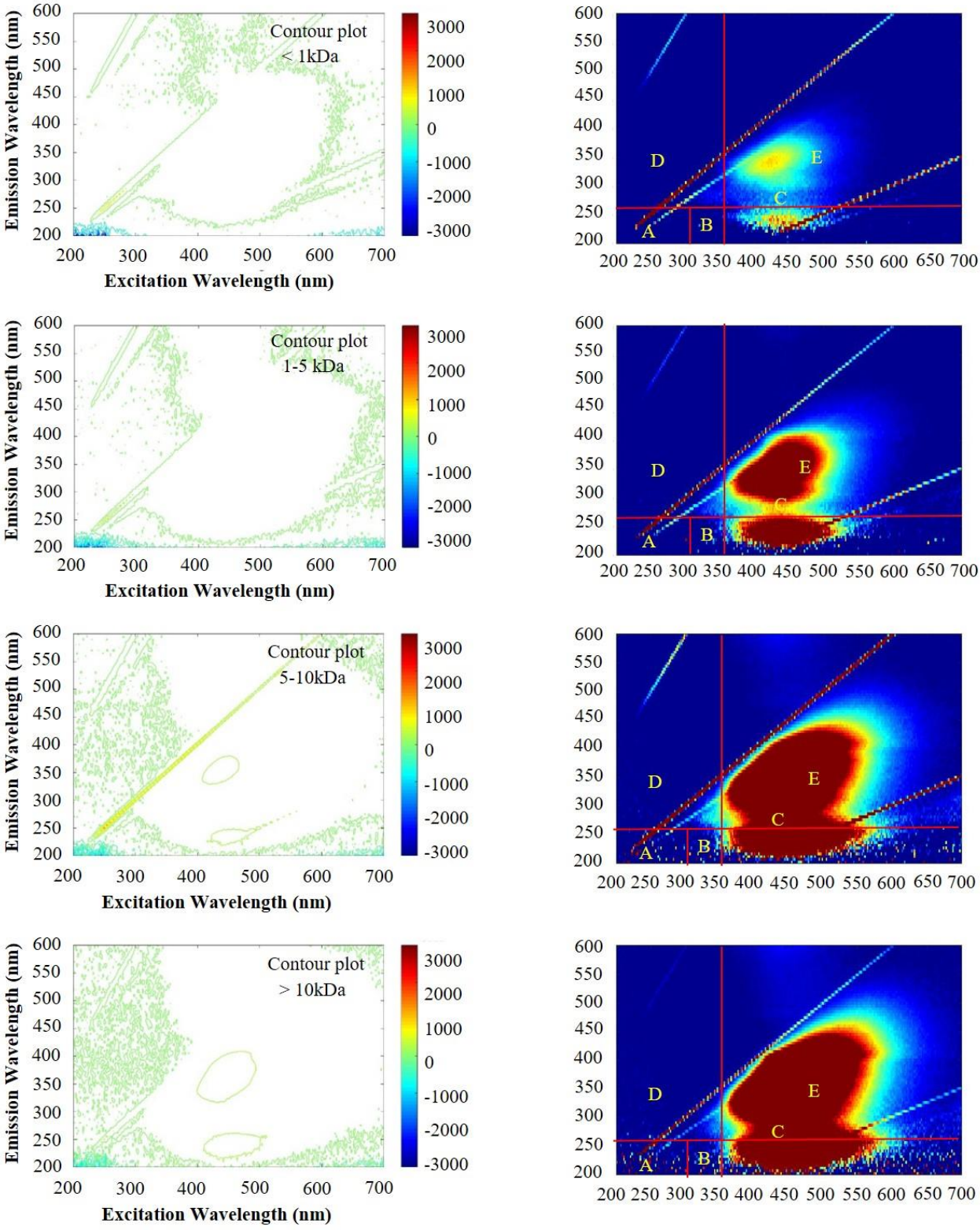

Figure 6 (continued) Contour and display image plots for fractioned melanodin

3.3 Melanoidin reduction efficiency

Figure 7 represents the effect of contact time on melanoidin adsorbed onto porous materials used in this study. Melanoidin adsorbed to the microporous material reached equilibrium at about 3.5 days and proceeded at low rates of adsorption for all molecular weight cut offs, depending on the order of >10kDa, 5-10kDa, 1-5kDa and <1kDa molecular weight fractions. All fractioned melanoidin adsorbed onto microporous material increased with time. It can be observed that the ability of adsorption onto melanoidin at different fractions had no significance on contact time. Owing to the interaction force and/or transport properties solid-liquid interface that influences the performances of pressure-driven processes between melanoidin and microporous adsorbent at different molecular weight cut off (MWCO) [51].

The melanoidin adsorbed to the mesoporous material was rapid to the equilibrium time of about Day 2.5, confirming that radius pore size distribution had affected the adsorption mechanism [52] of MWCO. It could be noticed that the amount of residual melanoidin adsorbed on mesoporous materials increased with time at different fractionations. However, the at <1kDa and >10kDa indicated the same mass of melanoidin adsorbed at equilibrium point in time were 12.56 mg melanoidin g^{-1} and 12.36 mg melanoidin g^{-1} at room temperature of about 25±0.05°C, respectively. The reason is that melanoidin at <1kDa molecular weight cut off had a radius porous equal to around 0.136 nm (1.36 Angstrom) that is less than the pore size of mesoporous materials (containing pores 2-50 nm in width or 20-50 Angstrom). Therefore, the capability of melanoidin adsorbed was only on the mesoporous surface diffusion, which did not show porous diffusion like monolayer adsorption and/or physical adsorption. While 5-10kDa (22.66 mg melanoidin g^{-1}) was a high melanoidin adsorbed as compared to other molecular weight cut off followed by 1-5kDa (20.98 mg melanoidin g^{-1}) was different of about 7.41% and 40.13% as compared to >10kDa and <1kDa, respectively. It might be that the permeate bulk protein concentration in the mixed synthetic melanoidin solution at different fractionations adversely affected the porous structure of materials used [53].

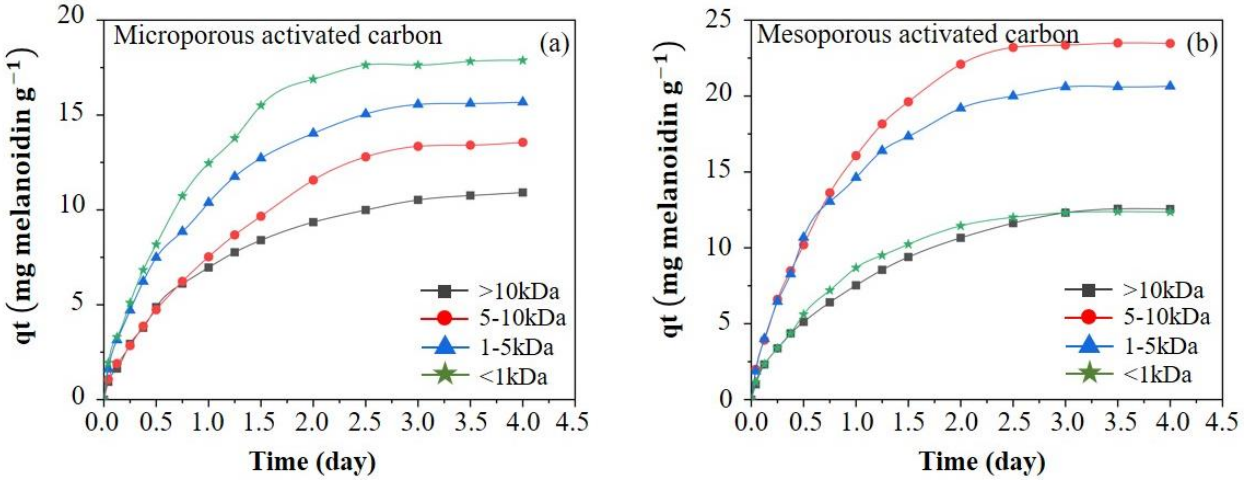

Figure 7 Effect of equilibrium time on a mass of melanoidin adsorbed at different fractionations onto micro- and mesoporous activated carbon

Figure 8 demonstrates equilibrium adsorption on a mass of melanoidin adsorbed at different fractionations onto micro- and mesoporous materials. Sorption studies of microporous materials were achieved whereas the melanoidins were highly adsorbed at a low molecular weight fraction of about <1kDa (17.88 mg melanoidin g^{-1}), following 1-5kDa (15.68 mg melanoidin g^{-1}), 5-10kDa (13.56 mg melanoidin g-1) and >10kDa (10.92 mg melanoidin g^{-1}), respectively. These confirmed that the molecular weight cut off had an effect on the adsorption process mechanism due to a mass balance transfer between solution bulk density concentration and the microporous surface.

In conditions under which mesoporous adsorbent, the mass of melanoidin adsorbed was high at the molecular weight cut off of about 5-10kDa (23.71 mg melanoidin g^{-1}), following 1-5kDa (20.63 mg melanoidin g^{-1}) and <1kDa (12.36 mg melanoidin g^{-1}) respectively. The >10kDa (12.56 mg melanoidin g^{-1}) showed less adsorption which might be due to size or the MWCO of melanoidin blocking the pores of the macroporous materials used (the pore diameter greater than 50 nm). In other words, it was observed that a different uniform concentration or isosurface between the melanoidin and macroporous materials used indicated the melanoidin was a well-fractioned bulk solution [54, 55] as visually confirmed in Figure 9.

Figure 9 gives the display image plots of before and after adsorption capacity for each fractionation adsorbed onto micro- and mesoporous materials through fluorescence spectroscopy.

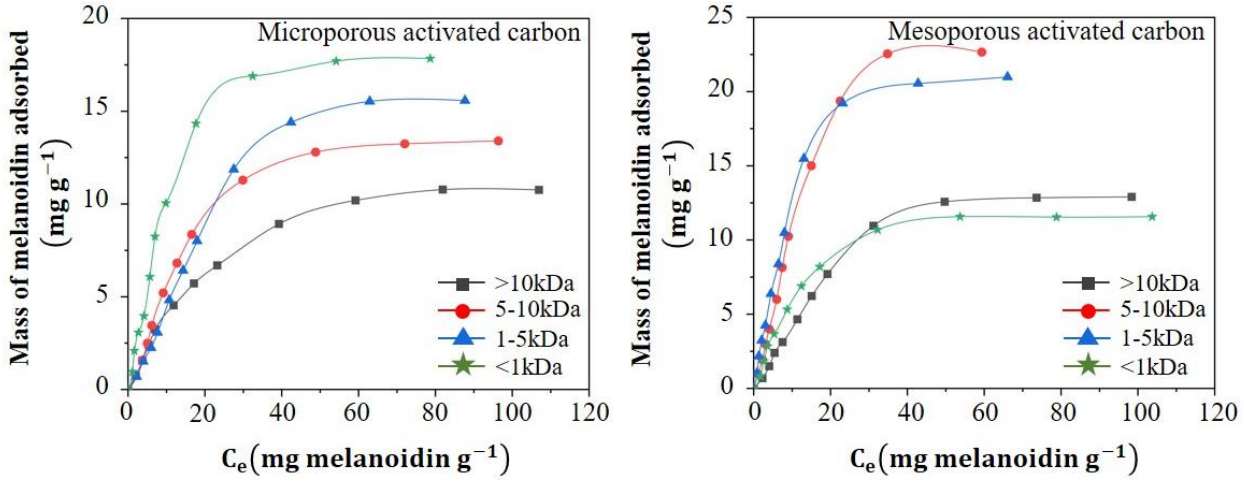

Figure 8 Sorption equilibrium on a mass of melanoidin adsorbed at different fractionations onto micro- and mesoporous activated carbon

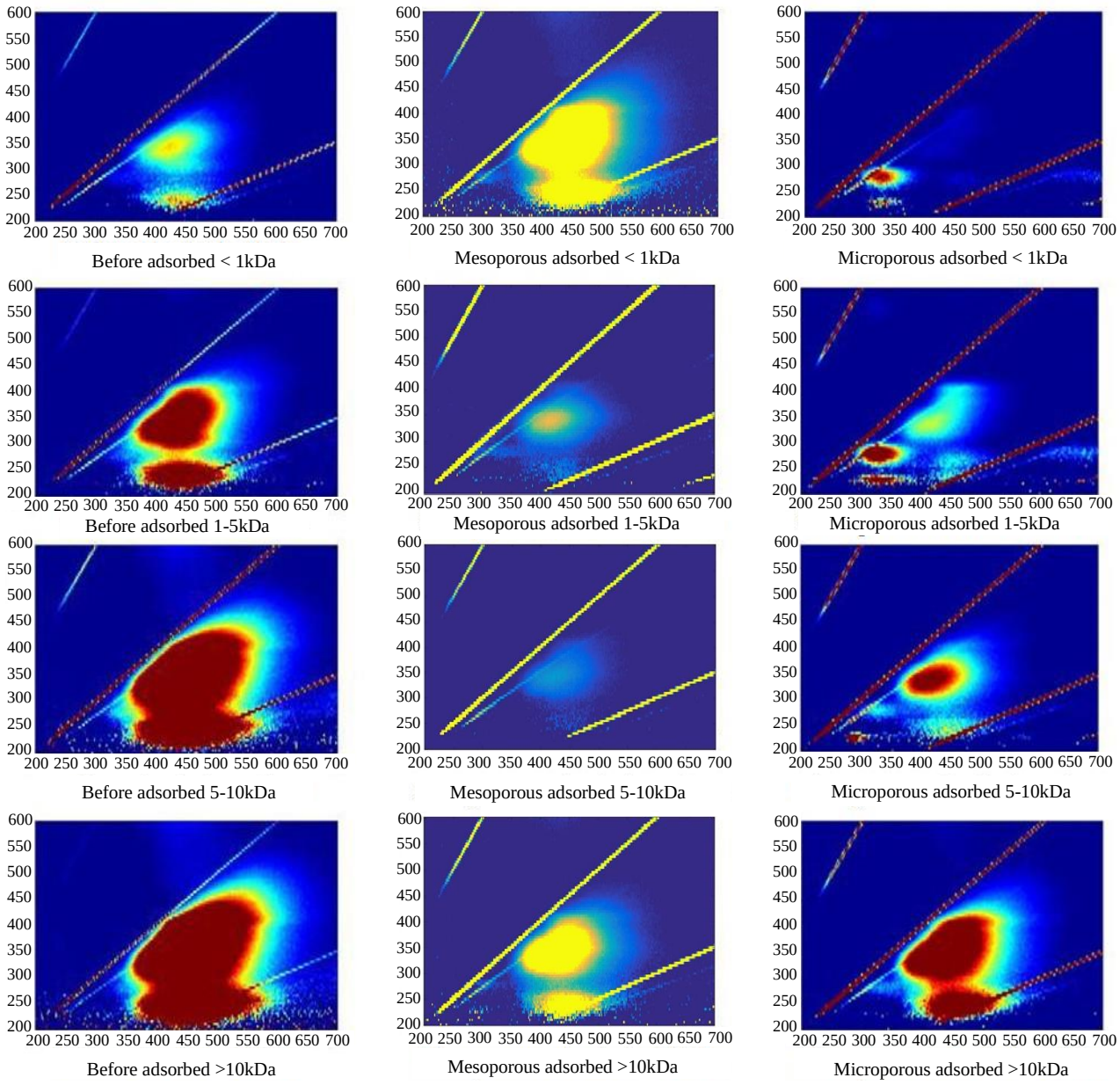

Figure 9 Display image plots before and after adsorption using fractioned melanoidin at different fractionations onto micro- and mesoporous activated carbon

Adsorption isotherms are curves that involve the variation amount of a solute concentration adsorbed on the surface or in the pores of an adsorbent at a given pressure, pH and temperature. To study the mechanism of adsorption between melanoidin and adsorbent at a constant temperature and pH, Langmuir and Freundlich were used to examine the mathematical analysis for process design. In nonlinear regression analyses, the experimental data is examined for the best fitting model using the statistical analysis of the Adjusted Coefficient of Determination (R^2_{adj}), Reduced Chi-Square (χ^2) and Residual Sum of Squares (RSS). Table 1 summarizes the results of regression analysis for the adsorption isotherm model obtained using nonlinear fitting for micro- and mesoporous activated carbon.

The comparison of the Langmuir and Freundlich isotherm models indicates that the Langmuir isotherm model provides the best statistical results for the Adjusted Coefficient of Determination, Reduced Chi-Square and Residual Sum of Squares as shown in Table 1 for both micro- and mesoporous materials used. It can be summarized that melanoidin adsorption onto adsorbent was limited to one molecular layer of non-interacting molecules, with chemisorption occurring at identical localized sites at or before a relative pressure of unity is reached. In other words, melanoidin adsorption was proportional to the fraction of the micro- and mesoporous surface, indicating the energetically largely homogeneous surface that was discussed in agreement with the basic feature of fractioned melanoidin and material characterization results. This finding was supported by the Freundlich isotherm parameter results and fitting plots (Figure 10), adsorption processes that affinities over the heterogeneous surface and heat of adsorption (multilayer adsorption). The Langmuir isotherm model provides a very good fit for a monolayer of adsorbed melanoidin onto the material surface that can be concluded form by physisorption. However, multilayers might occur at the first layer through chemisorption and the following layers through physisorption.

Figure 10 illustrates plots of isotherm data fitted to Langmuir and Freundlich at different fractionations. These image plots demonstrate that the best Langmuir isotherm model can provide good predictions, and the Freundlich isotherm model has less fit.

Table 1 Parameters of adsorption isotherm obtained using nonlinear fitting for melanoidin adsorbed onto micro- and mesoporous activated carbon at different fractionations

Carbon material	Model		Parameter	>10 kDa	5-10 kDa	1-5 kDa	<1 kDa
Microporous	Freundlich	$q_e = k_f \cdot C_e^{1/n_f}$	k_f (mg g^{-1})(L g^{-1})^n	1.4057	1.8461	1.3550	3.1712
			n_f	2.1633	2.1524	1.7250	2.3279
			$1/n_f$	0.4622	0.4646	0.5797	0.4296
			R^2_{adj}	0.9483	0.9064	0.9162	0.8971
			RSS	8.2232	24.3046	29.5289	47.2091
			χ^2	0.8223	2.4305	2.9529	4.7210
	Langmuir	$q_e = q_m \cdot k_l \frac{C_e}{1+k_l \cdot C_e}$	q_m (mg g^{-1})	13.81	17.40	24.34	22.16
			k_l (L mg^{-1})	0.0416	0.0477	0.0266	0.0774
			R^2_{adj}	0.9949	0.9785	0.9692	0.9797
			RSS	0.7956	5.5744	10.8428	9.3335
			χ^2	0.0796	0.5574	1.08435	0.0933
Mesoporous	Freundlich	$q_e = k_f \cdot C_e^{1/n_f}$	k_f (mg g^{-1})(L g^{-1})^n	2.2638	3.7084	2.7489	1.4918
			n_f	2.6119	2.2304	1.7994	1.9876
			$1/n_f$	0.3829	0.4484	0.5557	0.5031
			R^2_{adj}	0.8993	0.9010	0.9074	0.9064
			RSS	19.7682	61.0408	65.5419	23.1460
			χ^2	1.9768	6.1041	6.5542	2.3146
	Langmuir	$q_e = q_m \cdot k_l \frac{C_e}{1+k_l \cdot C_e}$	q_m (mg g^{-1})	13.8658	26.5263	33.9375	17.9722
			k_l (L mg^{-1})	0.0754	0.0818	0.0463	0.0359
			R^2_{adj}	0.9859	0.9810	0.9710	0.9724
			RSS	2.7724	11.9723	20.4927	6.8291
			χ^2	0.2772	1.1973	2.0493	0.6829

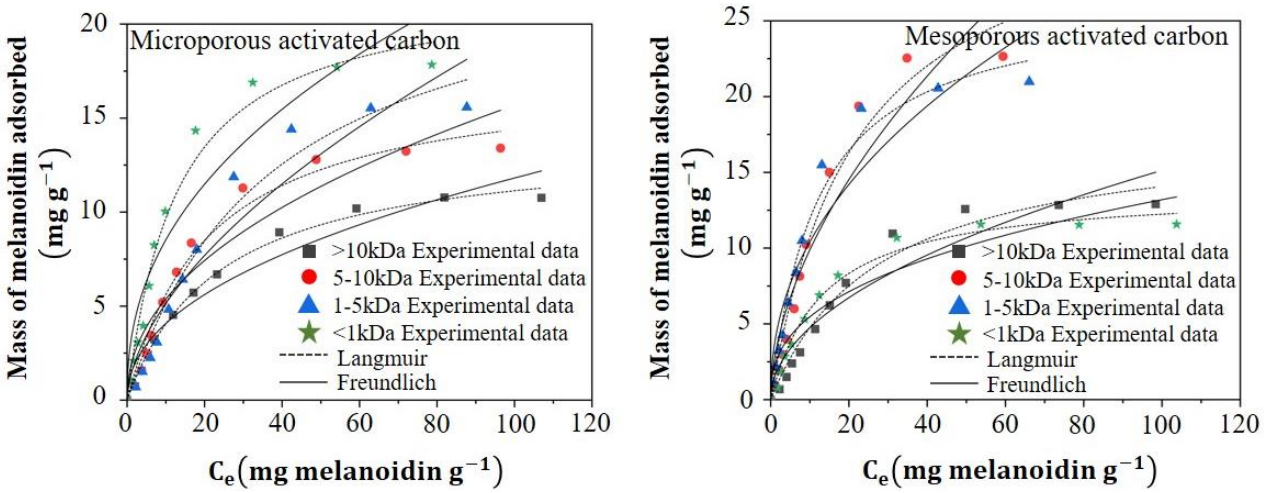

Figure 10 Langmuir and Freundlich isotherm plots of melanoidin adsorbed at different fractionations of >10kDa, 5-10kDa, 1-5kDa and <1kDa molecular weight fraction onto micro- and mesoporous materials

4. Conclusions

Serial fractionation using 10 kDa, 5 kDa and 1 kDa sterlitech ultrafiltration membranes was used to provide the characterization of wastewater associated with melatonin to prove a specific material in eliminating water pollutants. Results showed that the DOC, UV_{254} and $SSAC_{436}$ at different MWCO were higher for a higher molecular weight fraction in the order of 5-10kDa, 1-5 kDa and <1kDa respectively, with no specific change of pH around 7.54. The functional groups for each MWCO indicated multifunctional groups with distinguishing hydrogen bonds related to alcohol, phenols, carboxylic, alkynes and the alkyl amine group. It can be concluded that high MWCO can reflex with the IR-spectrum better than the low MWCO, in persisting of the peaks of fulvic acid-like materials and humic acid-like organic materials belonging to tryptophan and protein-like compounds. The equilibrium sorption performed in the nonlinear conditions of the Langmuir isotherm model gave an excellent fit, indicating monolayer coverage of adsorbed melanoidin onto the material surface. Sorption studies of microporous were achieved whereas the melanoidins were highly adsorbed at a low molecular weight fraction of about <1kDa (17.88 mg melanoidin g^{-1}), following 1-5kDa (15.68 mg melanoidin g^{-1}), 5-10kDa (13.56 mg melanoidin g^{-1}) and >10kDa (10.92 mg melanoidin g^{-1}), respectively. These confirmed that the MWCO affected the adsorption process mechanism due to a mass balance transfer between solution bulk density concentration and the microporous surface. The mesoporous adsorbent was observed that different uniform concentrations or isosurface of a component between melanoidin and macroporous materials used indicated the melanoidin was a well-fractioned bulk solution or due to pore size related to the filter's ability to filter out particles of a certain size.

These results suggest that the comprehensive characterization of artificial melanoidin can encourage the adsorbent materials in the removal of the remaining intractable organic pollutants that persist in wastewater discharge.

5. Acknowledgements

The authors would like to express their special thanks that this research was financially supported by Faculty of Engineering Mahasarakham University (Grant year 2021) and the University of Southern Queensland for providing financial support, the use of experimental equipment and the opportunity to complete this wonderful research work. This research was also supported by a Unit of Excellence (UOE64001) at the University of Phayao. Thanks also to the native English speaking editor who edited the English language in this paper prior to submission.

6. References

[1] Ames J, Wynne AG, Hofmann A, Kehraus S, Gibson GR. The effect of a model melanoidin mixture on faecal bacterial populations in vitro. Br J Nutr. 1999;82(6):489-95.
[2] Liang Z, Wang Y, Zhou Y, Liu H. Coagulation removal of melanoidins from biologically treated molasses wastewater using ferric chloride. Chem Eng J. 2009;152(1):88-94.
[3] Wongcharee S, Aravinthan V. Application of mesoporous magnetic nanosorbent developed from macadamia nut shell residues for the removal of recalcitrant melanoidin and its fractions. Sep Sci Technol. 2020;55(9):1636-49.
[4] Echavarria Velez AP, Pagan J, Ibarz A. Antioxidant activity of the melanoidin fractions formed from D-glucose and D-fructose with L-asparagine in the Maillard reaction. Sci Agropecuaria. 2013;4(1):45-54.
[5] Nunes FM, Coimbra MA. Role of hydroxycinnamates in coffee melanoidin formation. Phytochem Rev. 2010;9(1):171-85.
[6] Yaylayan V, Kaminsky E. Isolation and structural analysis of Maillard polymers: caramel and melanoidin formation in glycine/glucose model system. Food Chem. 1998;63(1):25-31.
[7] Benzing-Purdie LM, Cheshire MV, Williams BL, Sparling GP, Ratcliffe CI, Ripmeester JA. Fate of [15N] glycine in peat as determined by carbon-13 and nitrogen-15 CP-MAS NMR spectroscopy. J Agr Food Chem. 1986;34(2):170-6.
[8] Hirano M, Miura M, Gomyo T. Kinetic analysis of the inhibition by melanoidin of trypsin. Biosci Biotechnol Biochem. 1996;60(3):458-62.
[9] Simaratanamongkol A, Thiravetyan P. Decolorization of melanoidin by activated carbon obtained from bagasse bottom ash. J Food Eng. 2010;96(1):14-7.
[10] Chamy R. Biodegradation of hazardous and special products. London: IntechOpen; 2013.
[11] Fitzgibbon ML, Stolley MR, Kirschenbaum DS. An obesity prevention pilot program for African-American mothers and daughters. J Nutr Educ. 1995;27(2):93-9.
[12] Kannabiran B, Pragasam A. Effect of distillery effluent on seed germination, seedling growth and pigment content of *Vigna mungo* (L.) HEPPER (C.V.T.9). Geobios. 1993;20:108-12.
[13] Krishna Prasad R, Srivastava SN. Sorption of distillery spent wash onto fly ash: kinetics, mechanism, process design and factorial design. J Hazard Mater. 2009;161(2):1313-22.
[14] Gniechwitz D, Reichardt N, Ralph J, Blaut M, Steinhart H, Bunzel M. Isolation and characterisation of a coffee melanoidin fraction. J Sci Food Agr. 2008;88(12):2153-60.
[15] Chandra R, Bharagava RN, Rai V. Melanoidins as major colourant in sugarcane molasses based distillery effluent and its degradation. Bioresour Technol. 2008;99(11):4648-60.
[16] Mohana S, Desai C, Madamwar D. Biodegradation and decolourization of anaerobically treated distillery spent wash by a novel bacterial consortium. Bioresour Technol. 2007;98(2):333-9.
[17] Manisankar P, Viswanathan S, Rani C. Electrochemical treatment of distillery effluent using catalytic anodes. Green Chem. 2003;5(2):270-4.
[18] Dwyer J, Griffiths P, Lant P. Simultaneous colour and DON removal from sewage treatment plant effluent: alum coagulation of melanoidin. Water Res. 2009;43(2):553-61.
[19] Donyagard F, Zarei AR, Rezaei-Vahidian H. Application of magnetic carbon nanocomposites to remove melanoidin from aqueous media: kinetic and isotherm studies. Res Chem Intermed. 2017;43(8):4639-55.
[20] Wang Z, Shen L, Zhu S. Synthesis of core-shell Fe_3O_4@SiO_2@TiO_2 microspheres and their application as recyclable photocatalysts. Int J Photoenergy. 2012;2012(1):1-6.
[21] Groen JC, Peffer LA, Perez-Ramırez J. Pore size determination in modified micro-and mesoporous materials. Pitfalls and limitations in gas adsorption data analysis. Microporous Mesoporous Mater. 2003;60(1-3):1-17.
[22] Siderius DW, Gelb LD. Predicting gas adsorption in complex microporous and mesoporous materials using a new density functional theory of finely discretized lattice fluids. Langmuir. 2009;25(3):1296-9.
[23] Coluccia S, Marchese L, Martra G. Characterisation of microporous and mesoporous materials by the adsorption of molecular probes: FTIR and UV-Vis studies. Microporous Mesoporous Mater. 1999;30(1):43-56.
[24] Wongcharee S, Aravinthan V, Erdei L. Removal of natural organic matter and ammonia from dam water by enhanced coagulation combined with adsorption on powdered composite nano-adsorbent. Environ Tech Innovat. 2020;17:100557.
[25] Maretto M, Blanchi F, Vignola R, Canepari S, Baric M, Iazzoni R, et al. Microporous and mesoporous materials for the treatment of wastewater produced by petrochemical activities. J Clean Prod. 2014;77:22-34.
[26] Wang G, Otuonye AN, Blair EA, Denton K, Tao Z, Asefa T. Functionalized mesoporous materials for adsorption and release of different drug molecules: a comparative study. J Solid State Chem. 2009;182(7):1649-60.
[27] Sheng L, Zhang Y, Tang F, Liu S. Mesoporous/microporous silica materials: preparation from natural sands and highly efficient fixed-bed adsorption of methylene blue in wastewater. Microporous Mesoporous Mater. 2018;257:9-18.
[28] Wongcharee S, Aravinthan V, Erdei L. Mesoporous activated carbon-zeolite composite prepared from waste macadamia nut shell and synthetic faujasite. Chin J Chem Eng. 2019;27(1):226-36.
[29] Wang S, Li H. Structure directed reversible adsorption of organic dye on mesoporous silica in aqueous solution. Microporous mesoporous mater. 2006;97(1-3):21-6.
[30] Suwannahong K, Kreetachat T, Wongcharee S. Application of photocatalytic oxidation process using modified TiO2/PBS biocomposite film for dye removal. IOP Conf Earth Environ Sci. 2020;471:012013.
[31] Govindasamy C, Son WJ, Ahn WS. Synthesis of mesoporous materials SBA-15 and CMK-3 from fly ash and their application for CO 2 adsorption. J Porous Mater. 2009;16(5):545-51.

[32] Ello AS, de Souza LK, Trokourey A, Jaroniec M. Coconut shell-based microporous carbons for CO2 capture. Microporous Mesoporous Mater. 2013;180:280-3.
[33] Huang Q, Vinh-Thang H, Malekian A, Eic M, Trong-On D, Kaliaguine S. Adsorption of n-heptane, toluene and o-xylene on mesoporous UL-ZSM5 materials. Microporous mesoporous Mater. 2006;87(3):224-34.
[34] Masson S, Gineys M, Delpeux-Ouldriane S, Reinert L, Guittonneau S, Beguin F, et al. Single, binary, and mixture adsorption of nine organic contaminants onto a microporous and a microporous/mesoporous activated carbon cloth. Microporous Mesoporous Mater. 2016;234:24-34.
[35] Suwannahong K, Wongcharee S, Kreanuarte J, Kreetachart T. Pre-treatment of acetic acid from food processing wastewater using response surface methodology via Fenton oxidation process for sustainable water reuse. J Sustain Dev Energ Water Environ Syst. 2020;1080363.
[36] Cammerer B, Jalyschkov V, Kroh LW. Carbohydrate structures as part of the melanoidin skeleton. Int Congr. 2002;1245: 269-73.
[37] Wongcharee S, Aravinthan V, Erdei L, Sanongraj W. Mesoporous activated carbon prepared from macadamia nut shell waste by carbon dioxide activation: comparative characterisation and study of methylene blue removal from aqueous solution. Asia Pac J Chem Eng. 2018;13(7):e2179.
[38] Bernardo E, Egashira R, Kawasaki J. Decolorization of molasses' wastewater using activated carbon prepared from cane bagasse. Carbon. 1997;35(9):1217-21.
[39] Li D, Xie Y, Na X, Li Y, Dai C, Li Y, et al. Insights into melanoidin conversion into fluorescent nanoparticles in the Maillard reaction. Food Funct. 2019;10(7):4414-22.
[40] Chen J, Wang Q, Zhou J, Deng W, Yu Q, Cao X, et al. Porphyra polysaccharide-derived carbon dots for non-viral co-delivery of different gene combinations and neuronal differentiation of ectodermal mesenchymal stem cells. Nanoscale. 2017;9(30): 10820-31.
[41] Richard D, Nunez MD, Schweich D. Adsorption of complex phenolic compounds on active charcoal: breakthrough curves. Chem Eng J. 2010;158(2):213-9.
[42] Nguyen T, Fan L, Roddick F. Removal of melanoidins from an industrial waste water. Proceedings of OzWater 10 Conference; 2010 Mar 8-10; Brisbane, Australia. Brisbane: Australian Water Association; 2010. p. 1-6.
[43] Chen W, Westerhoff P, Leenheer JA, Booksh K. Fluorescence excitation-emission matrix regional integration to quantify spectra for dissolved organic matter. Environ Sci Tech. 2003;37(24):5701-10.
[44] Determann S, Reuter R, Wagner P, Willkomm R. Fluorescent matter in the eastern Atlantic Ocean. Part 1: method of measurement and near-surface distribution. Deep Sea Res Part I: Oceanogr Res Pap. 1994;41(4):659-75.
[45] Determann S, Reuter R, Willkomm R. Fluorescent matter in the eastern Atlantic Ocean. Part 2: vertical profiles and relation to water masses. Deep Sea Res Part I: Oceanogr Res Pap. 1996;43(3):345-60.
[46] Nguyen ML, Westerhoff P, Baker L, Hu Q, Esparza-Soto M, Sommerfeld M. Characteristics and reactivity of algae-produced dissolved organic carbon. J Environ Eng. 2005;131(11):1574-82.
[47] Sheng GP, Yu HQ. Characterization of extracellular polymeric substances of aerobic and anaerobic sludge using three-dimensional excitation and emission matrix fluorescence spectroscopy. Water Res. 2006;40(6):1233-9.
[48] Mounier S, Patel N, Quilici L, Benaim JY, Benamou C. Fluorescence 3D de la matiere organique dissoute du fleuve amazone: (Three-dimensional fluorescence of the dissolved organic carbon in the Amazon river). Water Res. 1999;33(6):1523-33.
[49] Ziegmann M, Abert M, Muller M, Frimmel FH. Use of fluorescence fingerprints for the estimation of bloom formation and toxin production of *Microcystis aeruginosa*. Water Res. 2010;44(1):195-204.
[50] Xin H, Tang Y, Liu S, Yang X, Xia S, Yin D, et al. Impact of graphene oxide on algal organic matter of *Microcystis aeruginosa*. ACS Omega. 2018;3(12):16969-75.
[51] Kadel S, Pellerin G, Thibodeau J, Perreault V, Laine C, Bazinet L. How molecular weight cut-offs and physicochemical properties of polyether sulfone membranes affect peptide migration and selectivity during electrodialysis with filtration membranes. Membranes (Basel). 2019;9(11):153.
[52] Suresh Kumar P, Korving L, Keesman KJ, van Loosdrecht MCM, Witkamp G-J. Effect of pore size distribution and particle size of porous metal oxides on phosphate adsorption capacity and kinetics. Chem Eng J. 2019;358:160-9.
[53] Xu Y, Sirkar KK. Protein mass transfer enhancement in the membrane filtration-cum-adsorption process. J Membr Sci. 2003;221(1):79-87.
[54] Asad A, Chai C, Wu J. Effect of protein molecular weight on the mass transfer in protein mixing. Sci China Phys Mech Astron. 2012;55(3):470-6.
[55] Doran PM. Bioprocess engineering principles. 2nd ed. London: Academic Press; 2013.